Short-Range Wetting at Liquid Gallium-Bismuth Alloy Surfaces: X-Ray Measurements and Square-Gradient Theory

Short-Range Wetting at Liquid Gallium-Bismuth Alloy Surfaces: X-ray measurements and Square-Gradient theory.

Patrick Huber* and Oleg Shpyrko, Peter S. Pershan
Department of Physics, Harvard University, Cambridge, MA 02138

Ben Ocko, Elaine DiMasi
Department of Physics, Brookhaven National Laboratory, Upton, NY 11973

Moshe Deutsch
Department of Physics, Bar-Ilan University, Ramat-Gan 52900, Israel
(Dated: April 22, 2003)

We present an x-ray reflectivity study of wetting at the free surface of the binary liquid metal alloy gallium-bismuth (Ga-Bi) in the region where the bulk phase separates into Bi-rich and Ga-rich liquid phases. The measurements reveal the evolution of the microscopic structure of the wetting films of the Bi-rich, low-surface-tension phase along several paths in the bulk phase diagram. The wetting of the Ga-rich bulk's surface by a Bi-rich wetting film, the thickness of which is limited by gravity to only 50 Å, creates a Ga-rich/Bi-rich liquid/liquid interface close enough to the free surface to allow its detailed study by x-rays. The structure of the interface is determined with Ångström resolution, which allows the application of a mean-field square gradient model extended by the inclusion of capillary waves as the dominant thermal fluctuations. The sole free parameter of the gradient model, the influence parameter κ, that characterizes the influence of concentration gradients on the interfacial excess energy, is determined from our measurements. This, in turn, allows a calculation of the liquid/liquid interfacial tension, and a separation of the intrinsic and capillary wave contributions to the interfacial structure. In spite of expected deviations from MF behavior, based on the upper critical dimensionality (D_u=3) of the bulk, we find that the capillary wave excitations only marginally affect the short-range *complete* wetting behavior. A *critical* wetting transition that is sensitive to thermal fluctuations appears to be absent in this binary liquid-metal alloy.

PACS numbers: 61.25.Mv, 61.30.Hn, 68.10.–m, 61.10.–i

I. INTRODUCTION

The concept of a wetting transition that was introduced independently by Cahn[1] and Ebner and Saam[2] in 1977 has stimulated a substantial amount of theoretical and experimental work[3–7]. Due to its critical character it is not only important for a huge variety of technological processes ranging from alloying to the flow of liquids, but has been proven to be an extraordinarily versatile and universal physical concept, which can be used to probe fundamental predictions of statistical physics. In particular, in the present case of wetting dominated by short-range interactions (SRW) it can be used, in principle, to probe the breakdown of mean-field behavior and the onset of the renormalization group regime, where the wetting is significantly affected by thermal fluctuations. In binary liquids having long-range interactions, e.g. van der Waals, which have been extensively studied[7], this is possible only near criticality, where the effects of wetting and criticality are intermixed and very difficult to separate.

A wetting transition occurs for two fluid phases in or near equilibrium in contact with a third inert phase, e.g., the container wall or the liquid-vapor interface. On approaching the critical point of coexistence the fluid phase that is energetically favored at the interface forms a wetting film that intrudes between the inert phase and the other fluid phase. In general, this surface phenomenon is a delicate function of both the macroscopic thermodynamics of the bulk phases and the microscopic interactions.

One of the seminal theoretical studies[2] on the wetting transition gave a detailed microscopic view of this phenomenon. By contrast, experimental results of comparable detail were only recently obtained through application of X-ray and neutron reflection and diffraction techniques[8–10]. Moreover, almost all of these experimental studies dealt with organic liquids, e.g. methanol-cyclohexane, which are dominated by long-range van-der-Waals interactions[7]. The principal exceptions to this are the studies of the binary metallic systems gallium-lead (Ga-Pb)[11], gallium-thallium (Ga-Tl)[12], and gallium-bismuth (Ga-Bi)[13], for which the dominant interactions are short-range.

We present here an x-ray reflectivity study of wetting behavior that occurs at the free surface of the binary metallic liquid Ga-Bi alloy at regions of the phase diagram where the bulk demixes into two liquid phases, a Bi-rich one and a Ga-rich one. The fact that the wetting film's thickness is limited by gravity to 50 Å allows measurements of the compositional profile of the wetting film at Ångström length scales. Moreover, the Ga-rich/Bi-rich liquid/liquid (l/l) interface created just 50 Å below

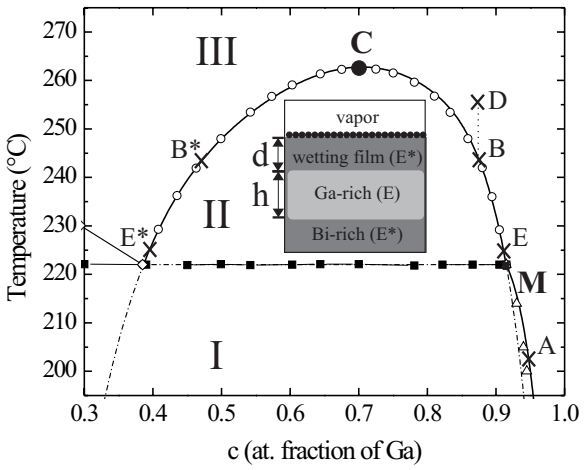

FIG. 1: The measured[14] (open circles and solid squares) bulk (c, T) phase diagram of Ga-Bi, where c is the atomic mole fraction of Ga, and T is the temperature. Solid lines show phase boundaries calculated from thermodynamical data[15]. Dashed lines show the metastable extension of the (l/l) coexistence line below $T_{\rm M}$. The points indicated are: C-bulk critical point, M-monotectic point, A,B,D,E-points on the experimental path. The crosses at B*, E* indicate the Bi-rich phases at the characteristic points B, E resp. The inset illustrate the surface and bulk phases. Roman numerals indicate regions discussed in the text. In region II the wetting film's thickness $d \approx 50$ Å and the Ga-rich fluid is $h \approx 5$ mm thick. The solid circles in the inset symbolize the Gibbs-adsorbed Bi-monolayer existing at the surface of the sample at all temperatures.

the free surface is also accessible to x-ray measurements. The structure of the film has been obtained as it evolves towards the saturation thickness determined by gravity. Combining this structural information and the bulk thermodynamics of the system, detailed information on the dominant interaction parameters governing the surface phenomenology have been extracted. We find that a square gradient theory[31] combined with the effects of thermally excited surface capillary waves[23,41,42] provides a reasonable description of that interface. In fact, we are able to determine the value of the sole free parameter of that model, the influence parameter κ. This parameter measures the influence of compositional gradients on the interfacial excess energy. This, in turn, allows a distinction to be made between the intrinsic (mean-field) and fluctuation (capillary waves) contributions to the interfacial structure. On the basis of this distinction the influence of fluctuations on the observed SRW at the free surface.

The paper is structured as follows: In the first section, we introduce the bulk phase diagram of Ga-Bi and relate its topology to the wetting transitions observable at the free surface of this binary alloy. X-ray reflectivity measurements on the wetting films along different paths in the bulk phase diagram are discussed in the second section. The third section focuses on the thermodynamics and structure of the liquid-liquid interface. In this section we develop a square gradient theory in order to model the concentration profile at the liquid/liquid interface. The last section provides a more general overview of the wetting phenomenology at the free surface of this binary liquid metal.

II. BULK & SURFACE THERMODYNAMICS

The bulk phase diagram of Ga-Bi, Fig. 1, was measured by Predel using differential calorimetry[14]. It is dominated by a miscibility gap with a consolute point C (critical temperature $T_C = 262.8°C$, critical atomic fraction of Ga, $c_{\rm crit} = 0.7$) and a monotectic temperature, $T_M = 222°C$. In region I, where $T < T_{\rm M}$, solid Bi coexists with a Ga-rich liquid. At $T_{\rm M}$, the boundary between region I and region II, a first order Bi melting transition occurs. For $T_{\rm M} < T < T_{\rm C}$ (region II), the bulk separates into two immiscible phases, a high density Bi-rich liquid and a low density Ga-rich liquid, over a range of concentrations c. The heavier Bi-rich phase is macroscopically separated from the lighter Ga-rich phase by gravity. In region III, outside of the miscibility gap, a homogeneous liquid is found.

Following the observation of Perepezko[16] that Bi-containing Ga-rich droplets are coated upon cooling by a Bi-rich solid phase, Nattland et. al.[13] studied the liquid-vapor interface in region II using ellipsometry. They found that a thin Bi-rich film intrudes between the vapor and the Ga-rich subphase in defiance of gravity[13], as shown by the layer marked E* in the inset in Fig. 1. This was a clear example of the critical point wetting in binary systems that was described by Cahn[1]. On approaching point C, the Bi-rich phase becomes energetically favored at the free surface and consequently forms the wetting film that intrudes between the Ga-rich subphase and the surface. In fact the situation is slightly more complicated since x-ray studies indicate that throughout region II the free surface is coated by a monolayer of pure Bi[17]. More recently we have shown by x-ray measurements[9] that a thick wetting layer of Bi-rich liquid forms between the Bi monolayer and the bulk Ga-rich liquid upon heating from below $T_{\rm M}$. This appears to be an unusual example of complete wetting that is pinned to the monotectic temperature $T_{\rm M}$. This phenomenon was first discussed by Dietrich and Schick in order to explain an analogous finding in the binary metallic alloy Ga-Pb[11,18]. The nature of this apparent coincidence of a surface wetting transition with a first order bulk transition at $T_{\rm M}$ can be understood most easily by transforming the (c, T)-diagram in Fig. 1 to the appropriate chemical potential-temperature (μ, T)-diagram, shown in Fig. 2(a). The axes are temperature, T, the difference $(\mu_{\rm Bi} - \mu_{\rm Ga})$ of the chemical potentials of the two components, and their sum $(\mu_{\rm Bi} + \mu_{\rm Ga})$. In this plot, the (l/l)-miscibility gap of Fig. 1, which,

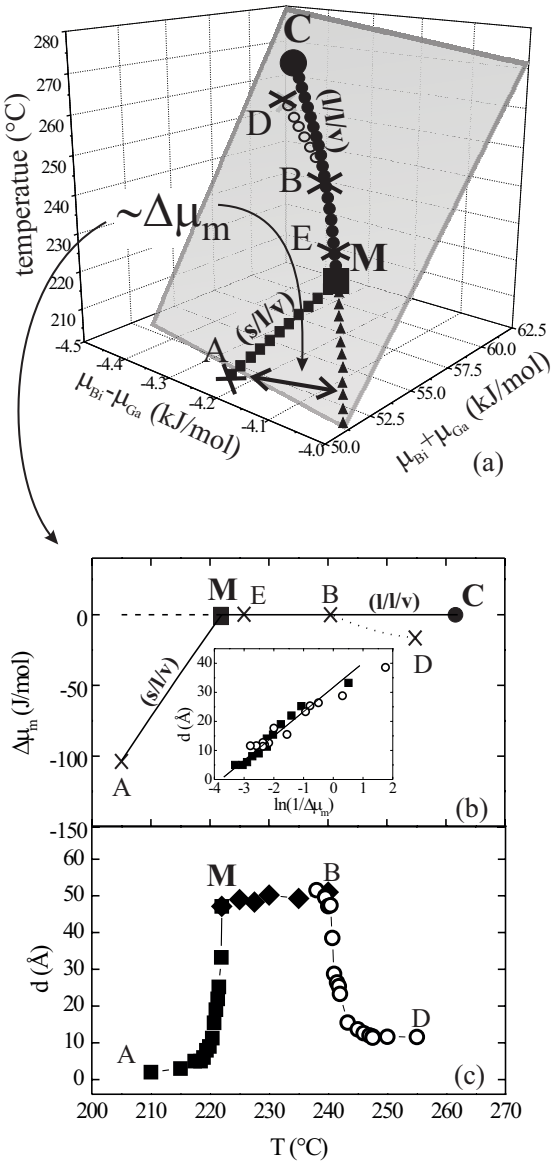

FIG. 2: **(a)** The chemical potential (μ)-temperature (T) bulk phase diagram of Ga-Bi. The axes are temperature, T, the difference ($\mu_{\rm Bi}-\mu_{\rm Ga}$) of the chemical potentials of the two components, and their sum ($\mu_{\rm Bi}+\mu_{\rm Ga}$). The solid symbols denote the following coexistence lines: •- liquid/liquid/vapor (l/l/v) triple line, ■-solid/liquid/vapor (s/l/v) triple line, ▲-metastable extension of the liquid/liquid/vapor (l/l/v) triple line below $T_{\rm M}$ and ∘-experimental path B-D probing complete wetting. The points are: C-bulk critical point of demixing, M-monotectic point, A,B,D,E-points on the experimental path. All these points are contained within a common liquid/vapor (l/v) coexistence sheet that is represented by a gray shaded plane in order to illustrate the three-dimensional structure of the phase diagram. The region to the lower right is the liquid/vapor coexistence, while the region to the left is the liquid/liquid coexistence. **(b)** The ($\Delta\mu_{\rm m}$,T) phase diagram: (A-M) and (M-C) are the (s/l/v) and (l/l/v) coexistence lines, respectively. The path B-D is in the single phase Region III of Fig. 1, and M and C are the monotectic and critical points. Inset: effective wetting layer thickness d on paths A→M (squares) and B→D (open circles). The solid line is a fit of the theoretical line discussed in the text to the measured A→M d-values. **(c)** The measured d values along the experimental path.

strictly speaking, is a liquid/liquid/vapor (l/l/v) coexistence boundary, transforms into a (l/l/v)-triple line extending from M to C (solid circles). At M this triple line intersects another triple line, the solid/liquid/vapor (s/l/v)-coexistence line (solid squares), rendering M a *tetra point* where four phase coexist:[73] a solid Bi, a Ga-rich liquid, a Ga-poor liquid, and the vapor.

The thermodynamics by which the surface transition at M is pinned by the bulk phase transition is obvious if one considers the topology of the (μ,T)-plot in the proximity of M. The wetting of the free surface by the Bi-rich phase as well as the bulk transition are driven by the excess free energy, $\Delta\mu_{\rm m}$, of the Bi-rich phase over that of the Ga-rich liquid phase[5]. This quantity is proportional to the distance between the (l/l/v)-triple line and any other line leading off (l/l/v)-coexistence, e.g. the (s/l/v)-triple line (A→M) or the line B→D. The wetting thermodynamics is displayed in a slightly simpler way by the plot of $\Delta\mu_{\rm m}$ vs. T in Fig. 2(b). In this figure, at $T > T_{\rm M}$, the (l/l/v) coexistence line transforms into a horizontal straight line that extends from M to C. For $T < T_{\rm M}$ the horizontal dashed line indicates the metastable (l/l/v) extension of the coexistence. This extension line lies above the solid-Bi/Ga-rich/vapor (s/l/v) coexistence line that goes from M to A. This illustrates the observation by Dietrich and Schick[18] that the path A→ M leads to coexistence, and thus complete wetting is dictated by the topology of the phase diagram.

A more quantitative description of the surface wetting phenomena can be developed by considering the grand canonical potential, $\Omega_{\rm S}$ per unit area A of the surface[5]: $\Omega_{\rm S}/A = d\,\Delta\mu + \gamma_0\, e^{-d/\xi}$. Here, d is the wetting film thickness, ξ is the decay length of a short-range, exponentially decaying surface potential, γ_0 is its amplitude and A is an arbitrary surface area. The quantity $\Delta\mu$ includes all the energies that are responsible for a shift off true bulk (l/l/v) coexistence, e.g. the aforementioned quantity $\Delta\mu_{\rm m}$. The formation of the heavier Bi-rich wetting layer at some height, h, above its bulk reservoir costs an extra gravitational energy $\Delta\mu_{\rm g}$=$g\Delta\rho_{\rm m}h$ where $\Delta\rho_{\rm m}$ is the mass density difference between the two phases. Minimization of $\Omega_{\rm S}$ with respect to d then yields the equilibrium wetting film thickness of the Bi-rich phase $d = \xi\ln(\gamma_0/\Delta\mu)$. In fact the gravitational energy is only significant in comparison with the other terms for very small values $\Delta\mu_{\rm m}$. For most of the data shown in Fig. 2 the gravitational term can be neglected, resulting in $\Delta\mu = \Delta\mu_{\rm m}$. Thus, upon approaching M from A one expects a logarithmic increase in the wetting film thickness that is given by $d = \xi\ln(\gamma_0/\Delta\mu_{\rm m})$. This is in agreement with the experimental findings presented in our recent Letter[19], shown also in the inset to Fig. 2(b) . The slight deviations at small values of $\Delta\mu_{\rm m}$, as well as the saturation value of $d \sim 50\mathring{A}$ when following the path M→B along the coexistence line, are due to the gravitational term. Since this path along the (l/l/v)-coexistence line ends in M with its four phase coexistence, the phenomenon is properly described as *tetra point wetting*. As

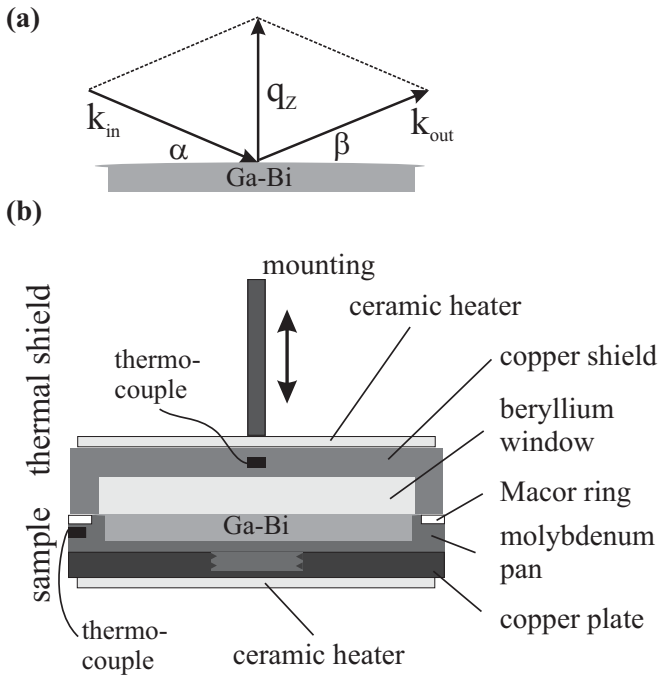

FIG. 3: (a) The scattering geometry (b) Sketch of the experimental setup. The arrow close to the mounting indicates the variable position of the thermal shield relative to the sample surface.

we demonstrate below, the occurrence of this complete wetting phenomenon at the surface is an intrinsic feature of the bulk phase diagram.

In this paper we present x-ray reflectivity measurements that show the evolution of the wetting film on approaching coexistence from point D in regime III. This path probes complete wetting along an arbitrary, off-coexistence path, B→D in Figs. 1 and 2(a,b), that is not dictated by the intrinsic topology of the bulk phase diagram. Rather, it is determined by the experimenter's choice of the total amounts of Ga and Bi in the sample, i.e. the nominal Ga concentration $c_{\rm nom}$. The evolution of the wetting film's structure along an on-(l/l/v)-coexistence path B→ E was also studied and is presented below.

III. EXPERIMENT

A. Sample Preparation & Sample Environment

The Ga-Bi alloy was prepared in an inert-gas glove box using > 99.9999% pure metals. A solid Bi pellet was covered by an amount of liquid Ga required for a nominal concentration $c_{\rm nom} = 88$ at% Ga. It was then transferred in air into an ultrahigh vacuum chamber. A 24-hour bakeout period yielded a pressure of 10^{-10} torr. The residual surface oxide on the liquid's surface was removed by sputtering with Ar^+ ions. Using thermocouple sensors and an active temperature control on both sample pan and its adjacent thermal shield a temperature stability and uniformity of ±0.05° C was achieved. Schematics of the x-ray reflectivity geometry and the sample cell are shown in Fig. 3(a,b).

The high surface tension of liquid metals, e.g. ≈700mN/m for pure Ga, presents a challenge for x-ray reflectivity measurements. To begin with, it leads to a curvature of the liquid surface which hampers x-ray reflectivity measurements[20]. It also considerably reduces the wettability of non-reacting substrates by the liquid metal. Remnant oxide layers at the liquid/substrate interface further reduce the wettability. We removed these oxide layers from the Mo sample pan by sputtering with Ar^+ ions, at a sputter current of 25mA and a sputter voltage of 2kV. This resulted in the wetting of the Mo crucible by the liquid metal, which yielded a rather small curvature for the free surface as judged by eye and by x-ray reflectivity measurements. The resulting flat surfaces facilitated the accumulation of reliable x-ray reflectivity data sets, particularly for small incident angles, α, where the x-ray beam's footprint on the surface is large. Nevertheless, the wetting of the edges of the Mo crucible by the liquid alloy promoted some spilling of the liquid when the experimental cell was moved during the reflectivity scan. This problem was solved by installing a ceramic (Macor) ring that surrounded the sample pan. Since ceramics are not wet by the liquid metal, sample spilling during movements was thus prevented.

Another experimental challenge is related to x-ray reflectivity measurements from liquids in general. The surface of a liquid is sensitive to vibrations and acoustic noise pickup from the environment. This, in turn, roughens the surface. The resultant great reduction in the reflected signal prevents the attainment of atomic-scale resolution. Thus, our UHV chamber was mounted on an active vibration isolation stage[20], which, as revealed by the x-ray reflectivity measurements, effectively eliminated vibrational pickup.

B. X-Ray Reflectivity

X-ray reflectivity measurements were carried out using the liquid surface reflectometer at beamline X22B at National Synchrotron Light Source with an x-ray wavelength $\lambda = 1.54$ Å. Background and bulk scattering were measured by displacing the detector out of the reflection plane by 0.3°, and subtracting the measured value from that measured in the reflection plane. The scattering geometry within the reflection plane is shown in Fig. 3(a). The intensity $R(q_z)$, reflected from the surface, is measured as a function of the normal component of the momentum transfer, $q_z = (4\pi/\lambda)\sin(\alpha)$, and yields information on the surface-normal structure of the electron density $\rho(z)$ through the formula[21]:

$$\frac{R(q_z)}{R_F(q_z)} = \left| \int \frac{1}{\rho_{\rm sub}} \frac{d\,\langle\rho(z)\rangle}{dz} e^{iq_z z} dz \right|^2 , \qquad (1)$$

where the angle brackets denote an average over the surface-parallel coherence area determined by the instrumental resolution and the atomic size[22,23]. The symbol R_F denotes the Fresnel reflectivity from an ideally flat and abrupt surface having the electron density of the Ga-rich liquid. The standard procedure for determining the electron density profile $\rho(z)$ from the measured reflectivity $R(q_z)$ is to construct a simple and physically meaningful mathematical model for $\rho(z)$, use Eq. 1 to calculate the corresponding $R(q_z)$, and fit it to the experimental $R(q_z)$, thus obtaining the parameter values determining $\rho(z)$[22,24].

To model $\rho(z)$, we employ a three-box model[9], where the upper box represents the Gibbs-adsorbed Bi monolayer, the second box represents the Bi-rich wetting film and the lower box represents the bulk liquid. Each box is represented by a ρ_{sub}-normalized density and a width. The quantity ρ_{sub} denotes the electron density of the Ga-rich subphase. In the simplest approximation the electron density profiles of the interfaces between the different phases are described analytically by three error-functions (erf) for the three interfaces: vapor/Bi monolayer, Bi monolayer/Bi rich film, Bi rich film/Ga rich bulk.

The first two interfaces describing the monolayer feature were remained unchanged in the presence of the Bi-rich film, while only the diffuseness of the Bi rich film/Ga rich bulk phase interface, σ_{obs}, was a variable parameter as a function of T. The model also included size parameters that describe the thickness of the two upper boxes. The box that describes the bulk sub-phase extends to infinity. During the fitting the thickness of the monolayer box was kept constant while the thickness of the Bi-rich film was allowed to vary.

The use of Eq. (1) tacitly assumes the validity of the Born approximation, where multi-scattering effects can be neglected[25]. This assumption holds true for wave vectors $q_z \gtrsim 4q_c \approx 0.2\text{Å}^{-1}$, where $q_c \approx 0.05\text{Å}^{-1}$ is the critical wavevector of the Ga-rich subphase. Here, however, we will be interested in 30-60 Å thick wetting films, which yield momentum-space features at $q_z \approx 0.05 - 0.1\text{Å}^{-1}$. Therefore, we use for $q_z >= 0.2$ Å^{-1} a fitting algorithm based on Eq. (1), whereas we employ a fitting procedure relying on the recursive, more computational intensive Parratt formalism[26] for $q_z <= 0.2\text{Å}^{-1}$ and thus for q_z close to q_c. In this formalism, one employs a 2×2 matrix that relates the amplitudes and phases for the incoming and outgoing waves on both sides of a slab of arbitrary dielectric constant[27]. For the present problem we approximate the above mentioned three-box profile by a large number of thinner slabs of equal width, the densities (heights) of which are chosen to follow the envelope of the analytic profile, as shown in fig. 4. Typically the number of slabs was of the order of 300.

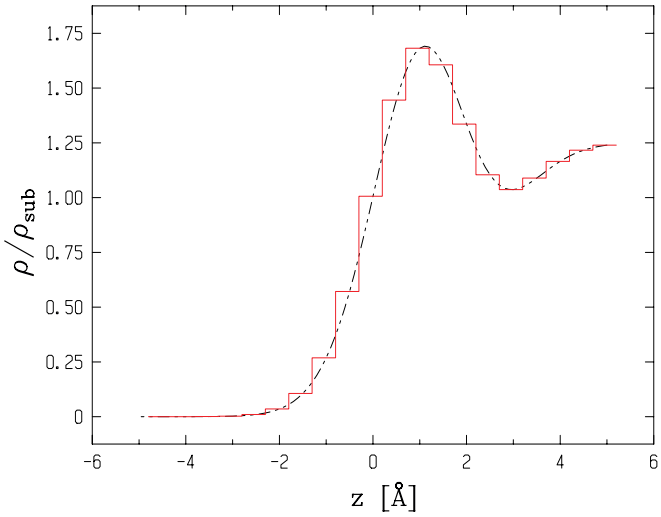

FIG. 4: An illustration of how a continuous, analytic electron density profile (dashed line) is approximated by a multislab model, which allows the use of the Parratt formalism. Only the region of the Bi-monolayer at the surface is shown.

IV. THE STRUCTURE OF THE WETTING FILM

A. Structure evolution off (l/l/v)-coexistence: The D → B path.

This path, in region III, and in particular its end point B, are determined solely by the overall atomic fraction of Ga in the sample pan, $c_{nom} = 88\%$. This nominal composition was chosen so that the intersection point B is far from the critical point C, where the electron density contrast between the Ga-rich and the Bi-rich liquid phases vanishes, but at the same time a long path on the (l/l/v) coexistence boundary is still possible before reaching point M. The intersection point B (see Figs. 1 and 2) is at $T_B = 240.4°$C, below which the homogeneous bulk liquid phase separates into the heavier Bi rich liquid, which settles to the bottom of the pan and the lighter Ga rich liquid, which stays on top.

X-ray reflectivity $R(q_z)$ was measured at selected temperatures on path D→B. To accommodate slow atomic diffusion processes,[28–30] small temperature steps of $0.5°C$ were taken, and equilibration was monitored by taking repeated reflectivity scans at each T. Typically, the measured reflectivity fluctuated wildly for a couple of hours, after which it slowly evolved to a stable equilibrium. The fits (lines) to these equilibrium R/R_F (points) are shown in Fig. 5(b), and on an enlarged scale at points B and D in Fig. 5(a). The corresponding $\rho(z)$ profiles are shown in Fig. 5(c). At point D ($T_D = 255°C$), typical of region III, R/R_F exhibits a broad peak at low q_z as well as an increased intensity around $q_z = 0.8$ Å^{-1}. The corresponding electron density profile $\rho(z)$, obtained from the fit, indicates a thin, inhomogeneous film of an increased electron density (compared to ρ_{sub}) close to the

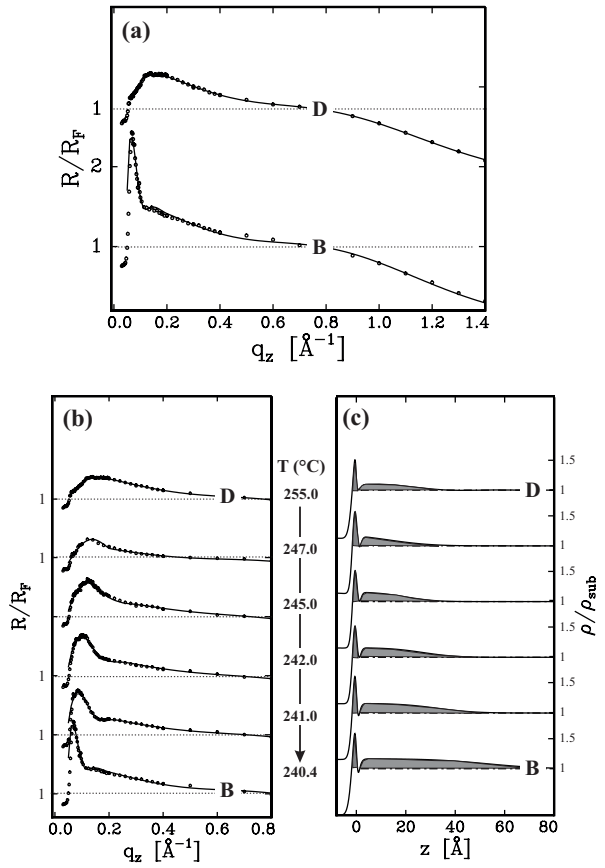

FIG. 5: **(a)** Fresnel-normalized reflectivities $R/R_{\rm F}$ at points D and B, corresponding to $T_{\rm D} = 255.0°$C and $T_{\rm B} = 240.4°$C. Curves are shifted vertically for clarity. The dashed lines indicate $R/R_{\rm F} = 1$. The error bars increase with increasing $q_{\rm z}$ but they are even at largest $q_{\rm z}$s only of the size of the data point symbols. **(b)** T-dependent Fresnel-normalized reflectivities $R/R_{\rm F}$ on path D →B, approaching (l/l) coexistence, along with their model fits. Dashed lines indicate $R/R_{\rm F} = 1$.**(c)** Electron density profiles $\rho/\rho_{\rm sub}$, corresponding to the model fits in (**b**). All regions with $\rho/\rho_{\rm sub} > 1$ (gray shading) indicate enrichment by Bi relative to the Bi concentration of the Ga-rich subphase.

surface as well as a sharp, narrow density peak right at the surface. This profile is consistent with the expected segregated monolayer of pure Bi at the surface, separated from the bulk by a thin wetting layer of a Bi-rich phase. As the temperature is decreased towards B, the low-$q_{\rm z}$ peak shifts gradually to lower $q_{\rm z}$ values and its width decreases, indicating that the wetting layer grows continuously in thickness upon approaching $T_{\rm B}$. This is in agreement with a thermodynamic path probing complete wetting: $\Delta\mu_{\rm m} \to 0$ on path D→B.

Our experimental data clearly indicate film structures dominated by sizeable gradients in the electron density, which contrasts with the frequently used "homogeneous slab" models, but is in agreement with theoretical calculations. These range from density functional calculations via square gradient approximations to Monte Carlo simulations for wetting transitions at hard walls[2,31,32]. Inhomogeneous profiles have also been observed experimentally in microscopically resolved wetting transitions for systems dominated by long-range van-der-Waals interactions[8,33]. Clearly detailed interpretation of the non-uniform density of the GaBi wetting films will require either a density functional analysis, or some other equivalent approach. Nevertheless, even a simple model approximating the wetting layer by a slab of thickness d allows a reliable determination of the surface potential governing this complete wetting transition. In order to do so, effective film thickness values d have been extracted from the $\rho(z)$ profile, using $d = \int_{z_{\rm s}}^{\infty}[\rho(z) - \rho_{\rm Ga-rich}]/[\rho_{\rm Bi-rich} - \rho_{\rm Ga-rich}]dz$. Here $z_{\rm s}$ is the top of the wetting film, and $\rho_{\rm Bi-rich}$, $\rho_{\rm Ga-rich}$ are the electron densities of the coexisting bulk liquid phases, calculated from the phase diagram[19]. In Fig. 2(b,c) we show plots of these d-values versus both T and $\Delta\mu_{\rm m}$. The last plot shows the expected logarithmic behavior and provides the values $\Phi = 43$ J/mol and $\xi = 5.4$ Å for the amplitude and decay length of the short-range surface potential, $\Phi\exp(-z/\xi)$, dominating the wetting effect[19]. Moreover, agreement between the (d,$\mu_{\rm m}$)-behavior along the path $D \to B$ and the data for the path A→M provides an experimental proof that both paths have the same thermodynamic character, i.e. they probe complete wetting: $\Delta\mu_{\rm m} \to 0$, as predicted by Dietrich and Schick[18] .

B. Structure evolution on (l/l/v)-coexistence: The B→ E path.

The $R/R_{\rm F}$ curves measured along the on-coexistence path $B \to M$ are shown in Fig. 6(a). The existence of two peaks at low $q_{\rm z}$ indicates the presence of a fully formed thick film (~ 50 Å). The solid lines indicate the best fit results corresponding to the real space profiles shown in Fig. 6(b). The best fit value for the maximum density of the thick film, $\rho/\rho_{\rm sub} = 1.20$, agrees well with the 1.21 calculated form the phase diagram at point B.

These results are also reasonably consistent with the gravity limited thickness expected for a slab of uniform density. Using $\xi = 5.4\mathring{A}$, $\gamma_0 = 400$mN/m and the known material constants that make up $\mu_{\rm m}$ (see table I below) the calculated value for $d = d_{\rm g} = \xi\ln(\gamma_0/\Delta\mu_{\rm g}) = 15.6\xi = 85$Å. In view of the fact that this estimate does not take into account the excess energy associated with concentration gradients across the interfaces some overestimation of $d_{\rm g}$ is not too surprising. Nevertheless, this rough calculation does show that the wetting film thickness is expected to be on a mesoscopic rather than on the macroscopic length scale that has been observed for similar wetting geometries in systems governed by long-range, dispersion forces[6].

Upon cooling from point B to M, the intensity of the first peak of $R/R_{\rm F}$ increases as expected due to the gradual increase of the electron density contrast $\rho/\rho_{\rm sub}$ that

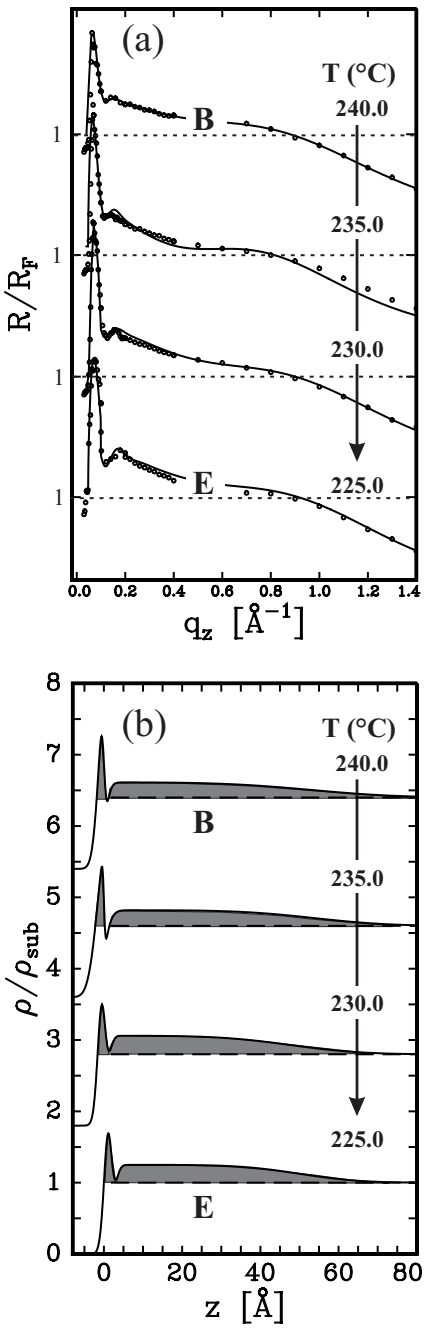

FIG. 6: **(a)** T-dependent, Fresnel-normalized reflectivities R/R_F measured on the on-coexistence path B→E along with their model fits. The error bars increase with increasing q_z but they are even at largest q_zs only of the size of the data point symbols. Dashed lines indicate $R/R_F = 1$. With increasing T, each R/R_F is shifted by 1.2. **(b)** Electron density profiles ρ/ρ_{sub} corresponding to the model fits in (**a**). All regions with $\rho/\rho_{sub} > 1$ (gray shading) indicate enrichment by Bi relative to the Bi concentration of the Ga-rich subphase.

follows from the increase in the Bi concentration in the bulk phase. Similarly, there is a small shift in the position of the peak indicating that the thickness varies slightly from 53 Å near B to 50 Å near E. This results from the T-dependence of the density contrast $\Delta\rho_m(T)$ as estimated from the bulk phase $\Delta\rho_m(T)$ listed in Table I. The on-coexistence path B→E is too far away from C to expect more pronounced effects on the wetting layer thickness due to a vanishing density contrast or the increase of the influence of the criticality on the interaction potentials[5,7,34].

Moreover the gravitationally imposed thickness limit on the on-coexistence wetting film to a length scale comparable to the range of the exponentially decaying short-range interactions prevents testing the influence of long-range, van-der-Waals-like atomic interactions on the wetting behavior that is present regardless of whether the system is metallic or not[35,36].

Finally, we would like to highlight the unique wetting geometry encountered here: The subtle balance between the surface potential that favors the Bi-rich liquid phase at the surface and the gravitational potential that favors the Ga-rich liquid phase above the denser Bi-rich phase, pins the (l/l) interface between the two coexisting phases the Bi-rich wetting film, 50$\mathring{A}$ thick, and the underlying Ga-Rich bulk close to the free surface. It is this property that makes it possible to study the structure of these wetting films. For example, the non-zero width of the interface between that film and bulk, σ_{obs}, is the cause of the decay of the Kiessig fringes at low q_z. This will be discussed further in the following section.

V. THE LIQUID/LIQUID INTERFACE

In this section, we discuss the microscopic structure of the (l/l) interface separating the gravitationally limited, Bi-rich wetting film from the Ga-rich subphase, and its evolution along the on-coexistence path $B \to E$. We first describe a simple square gradient theory for this interface and then extend it to include the effects of thermally excited capillary waves. Using this theory and our reflectivity measurements, we extract the (l/l)-interfacial profile and the (l/l) interfacial tension.

A. Square Gradient Theory

Assume that the concentration at the (l/l)-interface changes continuously and monotonically from the bulk concentration of the homogeneous Bi-rich phase, c^I, to the bulk concentration of the homogeneous Ga-rich phase, c^{II}, over a length scale which is much larger than the intermolecular distance. The excess free energy for the inhomogeneous region can be then expanded in the local variables $c(\overrightarrow{r})$ and $\bigtriangledown c(\overrightarrow{r})$[31]. The Gibbs free energy density cost within the interface can then be expressed in terms of a combination of a local function $g(c(\overrightarrow{r}, T)$ and a power series in $\bigtriangledown c(\overrightarrow{r})$[31,37–39]:

$$\widetilde{G} = N \int_V \left[g(c(\overrightarrow{r}), T) + \frac{1}{2}\kappa \left(\nabla c(\overrightarrow{r})\right)^2 + ... \right] dV \quad (2)$$

$T(^\circ C)$	$c^{\rm I}$	$c^{\rm II}$	$\Delta\rho$ m	$\rho/\rho_{\rm sub}(calc)$	$\rho/\rho_{\rm sub}(obs)$	q_c	d_g	d	$\sigma_{\rm obs}$	$\sigma_{\rm calc}$
225.0	0.39	0.91	2.30	1.24	1.25	0.0498	84.7	50	11.78	12.0
230.0	0.41	0.90	2.20	1.24	1.25	0.0499	84.9	51	14.2	13.3
235.0	0.43	0.89	2.09	1.22	1.22	0.0500	85.2	52	15.0	14.9
240.0	0.45	0.88	1.95	1.21	1.21	0.0502	85.5	53	17.5	17.25

TABLE I: Material parameters for the coexisting liquid phases as calculated from the bulk phase diagram and from the electron density profiles obtained from our fits to the measured $R/R_{\rm F}$ at selected temperatures T along the on-coexistence path B→E. The atomic fraction of Ga in the coexisting Bi-rich and Ga-rich liquid phases are $c^{\rm I}$ and $c^{\rm II}$, respectively. $\rho/\rho_{\rm sub}(calc)$ and $\rho/\rho_{\rm sub}(obs)$ denote the calculated and observed electron densities relative to that of the bulk.

where N is the number of molecules per unit volume. The first term in the integrand, $g(c(\overrightarrow{r},T)$, is the Gibbs free energy density of a volume element dV at a position $\overrightarrow{r}$ within a homogeneous solution of concentration $c(\overrightarrow{r},T)$. The second term is the leading term in the power series expansion. The coefficient κ is called the influence parameter and characterizes the effect of concentration gradients on the free energy. From first principles, it is related to the second moment of the Ornstein-Zernike direct correlation function and can be replaced by the pair-potential-weighted mean square range of the intermolecular interactions of the system[31]. Equation (2) can be regarded as the Landau-Ginzburg functional for this problem.

We neglect for now surface-parallel concentration variations and apply Eq. (2) to the surface-normal compositional profile $c(z)$ of the interface. Moreover, we assume that the concentration variations along z are small enough in order to justify a truncation of the power series after the second order term, $(\nabla c)^2$. This assumption leads to the square gradient approximation. The Gibbs free Energy of the system per unit area A , $\widetilde{G}/A$, is then given by:

$$\frac{\widetilde{G}}{A} = N\int_{-\infty}^{+\infty}\left[g(c(z)) + \frac{1}{2}\kappa\left(\frac{dc(z)}{dz}\right)^2\right]dz \qquad (3)$$

The interfacial tension $\gamma_{\rm ll}$ is defined as the excess energy per unit area A of this inhomogeneous configuration over the Gibbs free energy G of the homogeneous liquid of either one of the coexisting phases. Choosing the reference system as the homogeneous Bi-rich liquid where the concentration is $c^{\rm I}$, the surface tension can be written as:

$$\gamma_{\rm ll} = \frac{1}{A}\left[\widetilde{G}(c(z)) - G(c^{\rm I})\right] \qquad (4)$$

Within the square gradient approximation Eq. (3) this definition of $\gamma_{\rm ll}$ yields:

$$\gamma_{\rm ll} = N\int_{-\infty}^{+\infty}\left[\Delta g(c(z)) + \frac{1}{2}\kappa\left(\frac{dc(z)}{dz}\right)^2\right]dz \qquad (5)$$

where the grand thermodynamic potential $\Delta g(c)$ is given by

$$\Delta g(c(z)) = g(c(z)) - g(c^{\rm I}) \qquad (6)$$

It follows then from Eq. (5) that the interfacial tension is a functional of the concentration profile $c(z)$ at the interface. The equilibrium surface tension is obtained by minimizing this functional, which leads to the Euler-Lagrange equation:

$$\Delta g(c(z)) = \kappa\,\frac{d^2c(z)}{dz^2} \qquad (7)$$

This differential equation, with the boundary conditions of $c(z) = c^{\rm I}$ on one side of the interface and $c(z) = c^{\rm II}$ on the other, determines $c(z)$ uniquely. Direct integration yields:

$$z(c) = z_0 + \int_{c_0}^{c}\sqrt{\frac{\kappa}{\Delta g(c)}}\,dc \qquad (8)$$

where z_0 and c_0 are arbitrarily chosen origins for the position and the composition. Note that the integrand in Eq. (8) indicates that any characteristic length scale, e.g. the intrinsic width of the interfacial profile, $\sigma_{\rm intr}$, must scale as $\sqrt{\kappa}$. This result will be discussed further in Sec. V.B.

An attractive feature of this theory is that it relates the interfacial concentration profile to κ and $g(c(\overrightarrow{r},T))$ regardless of the theoretical basis by which $g(c(\overrightarrow{r},T))$ is derived. We use here the extended regular solution model, presented in the Appendix, to model the homogeneous free energy of the binary liquid metal, particularly that used to model its miscibility gap. The sole quantity required to calculate the (l/l) interfacial profile and tension in that case is the influence parameter κ[40]. The influence parameter can be extracted, therefore, from a fit of the theoretical expression to the measured profile. In particular, a choice of a particular value of κ, yields, through a solution of Eq. (7) or Eq. (8), a particular profile characterized by an intrinsic width $\sigma_{\rm intr}$, the value of which can be compared directly with the measured interfacial width $\sigma_{\rm obs}$. Results derived this way are listed in Table I and discussed in more detail in Section V.C below.

B. Capillary Wave Excitations at the (l/l) Interface

The formalism presented so far relies on a simple mean-field picture that neglects any thermal fluctuations at the

(l/l) interface. By contrast, a real experiment is sensitive not only to the intrinsic finite width of the interface, but also to its additional temperature-dependent broadening by thermally excited capillary waves. An intuitive, semiphenomenological approach to handle the interplay between the two contributions to the interfacial width was developed by Buff, Lovett, and Stillinger[41,42]. They regard the interface as a membrane under tension characterized by a "bare" interfacial energy $\gamma_{\rm ll}$, calculated in the previous sub-section. This membrane sustains a spectrum of thermally activated capillary wave modes the average energy of which is determined by the equipartition theorem to be $k_{\rm B}T/2$. Integration over the capillary wave spectrum yields the average mean square displacement of the interface (i.e. the r.m.s. amplitude of the capillary waves), $\sigma_{\rm cap}$, as[23,41,42]:

$$\sigma_{\rm cap}^2 = \frac{k_{\rm B}T}{4\pi\gamma_{\rm ll}(\kappa)} \ln \frac{q_{\rm min}}{q_{\rm max}} \qquad (9)$$

Here $q_{\rm max}$ is the largest capillary wave vector that can be sustained by the interface. For bulk liquids this is typically of the order of π/molecular diameter. Note, however, that it does not seem realistic to consider excitations with wavelengths smaller than the intrinsic interfacial width, $\sigma_{\rm intr}$, as surface capillary waves[46,47]. Thus, the upper cutoff of the capillary waves can be taken as $q_{\rm max} = \pi/\sigma_{\rm intr}$. The determination of q_{min} is slightly more complicated since it depends on whether the resolution is high enough to detect the long wavelength limit at which an external potential $v(z)$, such as either gravity or the van der Waals interaction with the substrate, quenches the capillary wave spectrum. If the resolution is sufficiently high then $q_{\rm min} = \pi/L_{\rm v}$ where $L_{\rm v}^2 = \gamma_{\rm ll}^{-1}\frac{\partial^2 v(z)}{\partial z^2}$. Otherwise, $q_{\rm min}$ is determined by the instrumental resolution as $q_{\rm min} = \Delta q_{\rm res} = \pi/L_{\rm res}$ where Δq_{res} is the projection of the detector resolution on the plane of the interface, and $L_{\rm res}$ is the corresponding length scale over which the surface fluctuations can be resolved. In our case $q_{\rm res}$ is significantly larger than $q_{\rm v}$ therefore, $q_{\rm min} = q_{\rm res} = 0.04$ Å.

The capillary wave amplitudes obey gaussian statistics, yielding an error function type profile for the average interfacial roughness[48]. The intrinsic profiles $c(z)$ are also well described by error function profiles. Thus, the two contributions to the interfacial width can be added in quadrature[48], yielding a total interfacial width, $\sigma_{\rm calc}$:

$$\sigma_{\rm calc}^2 = \sigma_{\rm intr}(\kappa)^2 + \sigma_{\rm cap}(\gamma_{\rm ll}(\kappa))^2 \qquad (10)$$

Since both $\sigma_{\rm intr}$ and $\sigma_{\rm cap}$ depend on κ, its value is determined self-consistently by the requirement that $\sigma_{\rm calc}$ agrees with the experimentally determined roughness $\sigma_{\rm obs}$.

C. The (l/l) intrinsic profile and interfacial tension

We carried out a self consistent calculation of κ for the observed (l/l) interface at point E, where $\sigma_{\rm obs}(E) \approx 12$Å. This was done by first solving the Euler-Lagrange Equation (7)[74] which yields the intrinsic $c(z)$ profile as depicted and compared with an erf-profile in Fig. 7(a). From that we calculated the corresponding intrinsic interfacial width $\sigma_{\rm intr}(E)$. Using the intrinsic $c(z)$ profile we numerically integrate Eq. (5) to obtain the interfacial tension $\gamma(E)$, and from that, using Eq. (9), we obtain the corresponding capillary-wave-induced roughness $\sigma_{\rm cap}$. The total width $\sigma_{\rm intr}$ is then calculated from Eq. (10). Starting with a reasonable value of κ , as judged by a scaling analysis of Eq. (7), this procedure was iterated until $\sigma_{\rm calc}(E) = \sigma_{\rm obs}(E)$ was obtained. This procedure yielded $\kappa_{\rm opt} = 5.02 \cdot 10^{-13}$ Nm^3/mol, $\sigma_{\rm cap}(E) = 10.32\mathring{A}$, $\sigma_{\rm intr}(E) = 6.35\mathring{A}$ and $\gamma_{\rm ll}(E) = 3.3$mN/m.

Note that Eq. (7) implies that $\sigma_{\rm intr} \propto \sqrt{\kappa}$, whereas Eq. (9) implies that $\sigma_{\rm cap} \propto \frac{1}{\sqrt{\kappa}}$. Hence, $\sigma_{\rm calc}(\kappa)$ should exhibit a minimum for $\sigma_{\rm calc}$ at some characteristic value, $\kappa_{\rm min}$. The $\kappa_{\rm opt}$ determined from our measurements corresponds to this peculiar value $\kappa_{\rm min}$. This means that the system "selects" from all possible ($\sigma_{\rm intr}$, $\sigma_{\rm cap}$) combinations the one which renders the overall width of the (l/l) interface minimal.

Assuming a T-independent influence parameter and using the thermochemical data available for a large part of the phase diagram, the T-dependent interfacial profiles and (l/l) interfacial tension can be calculated from a very low to a very high T, close to $T_{\rm C}$. The intrinsic (l/l) interfacial profiles calculated this way are plotted in Fig. 7(b) for selected T's versus the reduced temperature, $t = |\mathcal{T} - \mathcal{T}_{\rm C}|/\mathcal{T}_{\rm C}$ (Here and in the following $\mathcal{T}$ denotes the absolute temperature in Kelvin units). The increase in the width of the interface upon approaching $\mathcal{T}_{\rm C}$ ($t \to 0$) is clearly observed. The predicted rise of $\sigma_{\rm calc}$ over the investigated T-range, however, is rather small, just beyond the error-bars attributed to the measured $\sigma_{\rm obs}$. This precludes a more detailed quantitative analysis. Nevertheless, our measurements suggest an increase of $\sigma_{\rm obs}$ while increasing T in agreement with our model. The calculated t-dependence of the interfacial tension are in very good agreement with the experiment as shown in Fig. 9. As expected, $\gamma_{\rm ll}(T)$ vanishes as $t \to 0$.

Comparison of the $\gamma_{\rm ll}(T)$ values derived above with independent (preferably direct) measurements of this quantity would constitute a stringent test for the validity of the interpretation presented here for our measurements. Unfortunately, direct measurements of $\gamma_{\rm ll}(T)$ are rather difficult and we are not aware of any such measurements for Ga-Bi in the literature. It is, however, possible to estimate $\gamma_{\rm ll}(T)$ indirectly, using other experimental data on this alloy. For example, Predel[14] noted that in the vicinity of the critical point C the (l/l)-coexistence curve of Ga-Bi can be represented by $|\phi_{\rm c} - \phi| = K(T_{\rm c} - T)^{\beta}$ with $\beta \approx 0.33$, where ϕ is the volume fraction of either Ga or Bi and K is a constant[14]. This behavior suggests that the demixing transition in Ga-Bi belongs to the same universality class as nonmetallic binary liquid mixtures, i.e. to the Ising lattice model with dimensionality D=3. Moreover, it indicates that the two-scale-factor univer-

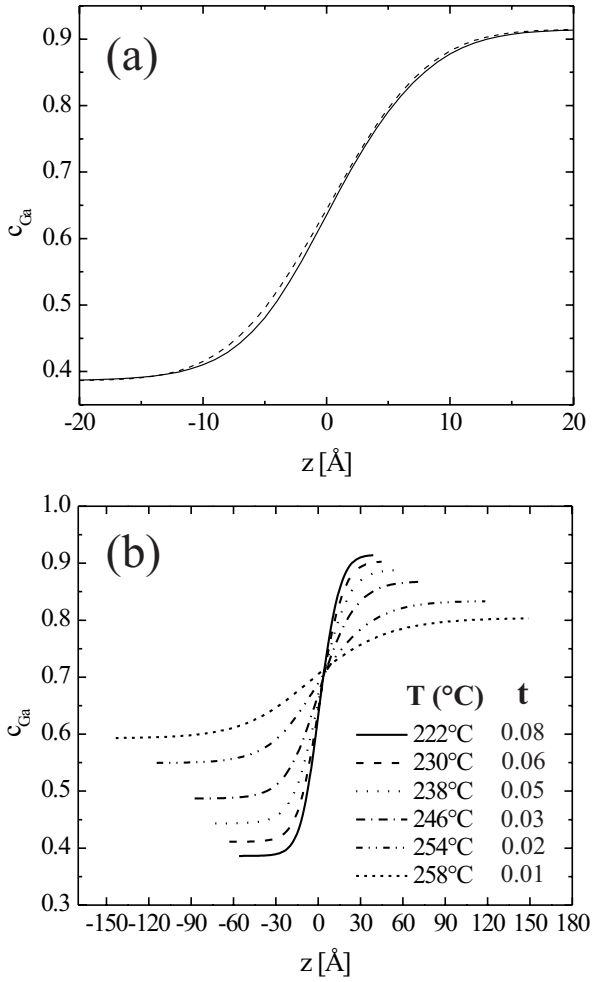

FIG. 7: **(a)** Calculated intrinsic profile $c(z)$ (solid line) at $T = T_{\rm E} = 225°{\rm C}$ ($t = 0.07$) approximated by an error-function profile (dashed line): $c(z) = \frac{c^{\rm I}+c^{\rm II}}{2} + \frac{(c^{\rm II}-c^{\rm I})}{2}\ {\rm erf}\left(\frac{z}{\sqrt{2}\sigma_{\rm intr}(E)}\right)$ with $\sigma_{\rm intr}(E) = 6.35$Å. **(b)** Calculated intrinsic concentration profiles $c(z)$ for the temperatures T (and corresponding reduced temperatures t) listed in the figure.

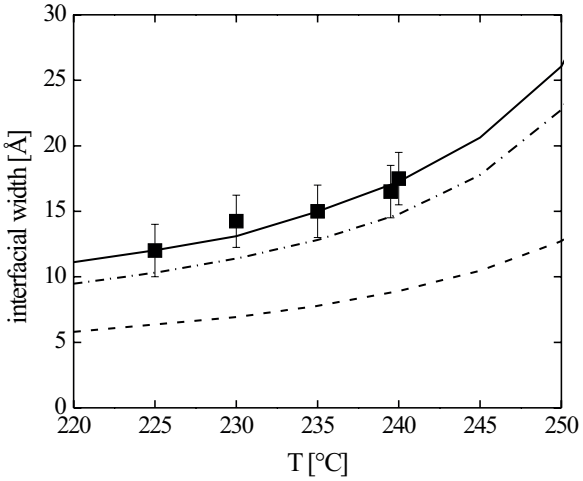

FIG. 8: Comparison of the temperature dependent measured interfacial width σ (■) with the calculated interfacial widths (lines): $\sigma_{\rm calc} = \sqrt{\sigma^2_{\rm intr} + \sigma^2_{\rm cap}}$ (solid) , intrinsic width $\sigma_{\rm intr}$ (dash-dot), and capillary width $\sigma_{\rm cap}$ (dashed).

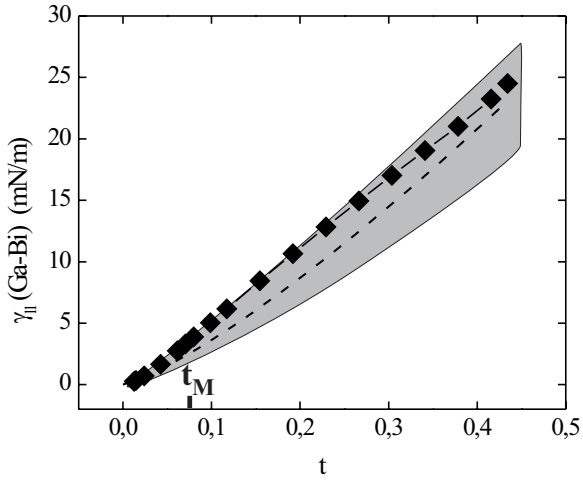

FIG. 9: The (l/l) interfacial tension $\gamma_{\rm ll}$ of Ga-Bi vs. the reduced temperature t, as calculated from our measurements using the square gradient theory (solid squares plus solid line). The dashed line is the TSFU prediction for Ga-Bi. The gray strip illustrates the error in the TSFU prediction[50]. The symbol $t_{\rm M}$ indicates the monotectic temperature at $t_{\rm M}$(Ga-Bi)= 0.08.

sality (TSFU)[49] theory should be valid for our system, which allows us to estimate the (l/l) interfacial tension from scaling relations. Using this concept along with available T-dependent measurements of the specific heat, Kreuser and Woermann extracted an expression for the T-dependent interfacial tension in Ga-Bi[50], $\gamma_{\rm ts} = \gamma_{\rm ts0}\ t^{\mu}$, where $\mu \approx 1.26$ is a critical exponent for the bulk demixing transition, and $\gamma_{\rm ts0} = 66 \pm 15$mN/m. The corresponding t-dependent $\gamma_{\rm ts}$ is plotted in a dashed line in Fig. 9. A very good agreement is observed with the t-dependence of $\gamma_{\rm ll}$ as calculated from our square gradient theory, considering the error bar of our results, shown by the gray strip. At point E, for example, where $t_{\rm E} = 0.07, T_{\rm E} = 225°{\rm C}$ we obtain $\gamma(E) = 3.31$mN/m, while $\gamma_{ts}(E) = 2.3$mN/m.[75]

D. The (l/l) interfacial tension of Ga-Pb

Aside from the Ga-Bi system, the Ga-Pb mixture is the only other metallic system for which detailed temperature dependent measurements[51] and estimations[52] of the (l/l) interface are reported in the literature. Given

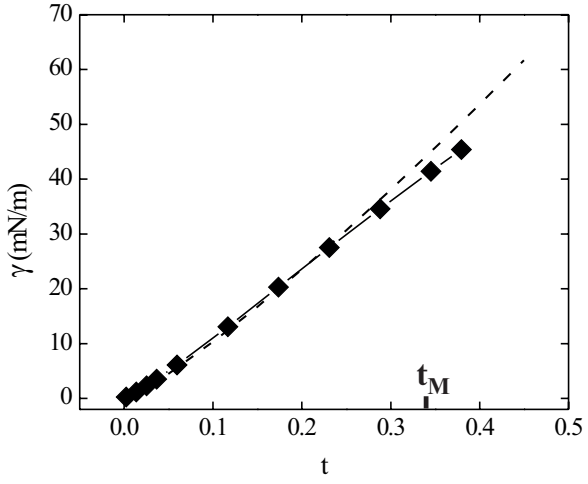

FIG. 10: Calculated (l/l) interfacial tension $\gamma_{\rm ll}$ of Ga-Pb as a function of the reduced temperature t. The solid points are our calculated values. The dashed line represents a fit to the measurements of Merkwitz et. al.[51]. The symbol $t_{\rm M}$ indicates the monotectic temperature at $t_{\rm M}$(Ga-Pb)= 0.33.

the similarities between Ga-Bi and Ga-Pb (similar constituents, identical phase diagram topology with a consolute point C and a monotectic point M), it is reasonable to assume that our gradient theory should be applicable to this binary system as well. Moreover, the influence parameter, κ, determined here for Ga-Bi, should be a reasonable approximation for κ of Ga-Pb. Published thermochemical data for the miscibility gap of Ga-Pb[53] allowed us to calculate the t-dependent (l/l) interfacial tension, $\gamma_{\rm ll}$, shown in Fig. 10. An excellent agreement is observed between these calculations and the measurements of Merkwitz et al.[51].

Overall, these results suggest that our model of an intrinsic, mean-field interface of a non-zero width broadened by capillary waves describes the (l/l) interface reasonably well. One must, however, bear in mind the approximations implicit in the analysis presented. For instance, we have assumed that the free surface of the liquid alloy behaves like a rigid wall, whereas in practice it has its own spectrum of capillary waves that could be coupled to the capillary waves at the (l/l) interface. However, since the interfacial tension of the free surface is about two orders of magnitude larger than the (l/l) interfacial energy in this metallic system, we believe that the rigid wall assumption is a reasonable approximation for our system. Furthermore, the calculation presented above assumes a T-independent influence parameter κ. While the agreement shown in Fig. 8 supports this assumption in our case, this may not be necessarily true for real fluids for all temperatures. In fact, the theory predicts that for real fluids κ diverges for $T \to T_{\rm C}$ as $\kappa \approx (T - T_{\rm C})^{-0.02}$, a divergence necessary in order to obtain the correct scaling behavior of $\gamma_{\rm ll}(T)$ near C[54–56].

VI. WETTING PHENOMENOLOGY AT THE FREE SURFACE

A. Effects of Fluctuations on Short-Range Wetting

Our analysis in Section III of the complete wetting transition at B was based on a mean-field (MF) model for a SRW transition. This model accurately predicts the critical behavior (i.e. the critical exponents) of systems close to a phase transition, only if fluctuations can be neglected. For SRW transitions, however, it can be shown that the upper critical dimensionality $D_{\rm u} = 3$[57]. The value $D_{\rm u}$ is the dimension beyond which MF theory can be applied successfully. If the dimension is smaller than $D_{\rm u}$ fluctuations are important and one has to resort to renormalization group (RG) methods to describe the critical behavior. For SRW, the upper critical dimensionality is exactly 3, implying that a 2D surface is expected to deviate from the MF behavior. Thus, the SRW transition has received a great deal of theoretical attention, since it allows one to explore the regime where the MF behavior breaks down due to fluctuations, and the RG approach becomes applicable. This break-down depends on the so-called fluctuation parameter, $\omega = k_{\rm B} \cdot \mathcal{T}/(4\pi\gamma_{\rm ll}\xi_{\rm b}^2)$, where $\xi_{\rm b}$ is the bulk correlation length, and $\gamma_{\rm ll}$ is the (l/l) interfacial tension. ω measures the magnitude of the dominant thermal fluctuations at the unbinding interface. These are in our case the thermally induced capillary waves at the (l/l) interface of the coexisting Bi- and Ga-rich liquids.

The RG analysis of the wetting transition yields the same logarithmic divergence for the wetting layer's thickness d as the MF analysis, discussed in Section II above. The only change is in the prefactor: $d_{\rm RG} \sim \xi_{\rm RG}\,(1 + \omega/2)\,\ln\,(1/\Delta\mu)$[5,58,59]. Using the bulk correlation length, $\xi_{\rm b}$ estimated from the TSFU analysis above, yields for the wetting transitions at M $\omega_{\rm M} = 0.3 \pm 0.2$ and for the observed complete wetting transition at B $\omega_{\rm B} = 0.4 \pm 0.2$. Thus, the prefactors of the logarithmic divergence law within the RG approach change at these points by only $\approx$ 10% and 20%, respectively, from their mean-field values. This is well within our experimental error of about 30% for the determination of ξ.[76]. We conclude therefore that a clear distinction between RG and MF behavior cannot be drawn in our case.

A *critical* wetting transition, where the wetting film forms, with a similar value of ω, at on-(l/l/v)-coexistence, rather than at (l,l)-coexistence only, should show a more pronounced deviation between MF and RG behaviors. Thus, we now proceed to estimate the characteristic wetting temperature $T_{\rm W}$ for that transition.

B. The Critical Wetting Transition in Ga-Bi

It follows from our measurements that the critical wetting transition has to be hidden in the metastable range of the (l/l/v) coexistence line somewhere below $T_{\rm M}$. An estimation of $\mathcal{T}_{\rm W}$ is possible by considering the spreading energy, $\Theta(\mathcal{T})$, which measures the free energy difference between the wet (Bi-rich wetting phase at the surface) and the non-wet (Ga-rich phase at the surface) situations at any temperature. Since the interfacial structure in the wet situation differs from that of the non-wet situation by the existence of an extra liquid-liquid interface, $\Theta(\mathcal{T})$ can be written as :

$$\Theta(\mathcal{T}) = \Gamma(\mathcal{T}) - \gamma_{\rm ll}(\mathcal{T}) \tag{11}$$

where $\Gamma(\mathcal{T}) = \gamma({\rm Ga-rich})_{\rm lv}(\mathcal{T}) - \gamma({\rm Bi-rich})_{\rm lv}(\mathcal{T})$ is the difference between the bare liquid-vapor surface tensions, $\gamma_{\rm lv}(\mathcal{T})$, of the two coexisting liquids. ¿From this definition of $\Theta(\mathcal{T})$ it follows that the formation of the wetting film is energetically favored for $\Theta > 0$ (wet-situation), whereas for $\Theta < 0$ it is unfavorable (non-wet situation). The condition $\Theta(\mathcal{T}) = 0$ marks, therefore, the transition temperature $\mathcal{T}_{\rm W}$, where the system switches on-coexistence between the non-wet and wet situations.

To estimate $\Theta(\mathcal{T})$, we need in addition to $\gamma_{\rm ll}(\mathcal{T})$, which was obtained in the previous section, also the values of $\gamma({\rm Ga-rich})_{\rm lv}(\mathcal{T})$ and $\gamma({\rm Bi-rich})_{\rm lv}(\mathcal{T})$. Measurements of these quantities are reported in the literature[60–62], the most recent one of which is that by Ayyad and Freyland[61,62], employing the noninvasive method of capillary wave spectroscopy. From these measurements, we get a conservative $\mathcal{T}$-independent estimate for Γ of the order of 100mN/m. Our calculation of $\gamma_{\rm ll}(\mathcal{T})$, particularly its extrapolation towards very low temperatures, $t \to 1$, which yields $\gamma_{\rm ll}(0{\rm K}) = 75{\rm mN/m}$, indicates that it is always significant smaller than Γ. Our analysis suggests, therefore, that $\Theta(\mathcal{T}) > 0$ for all $\mathcal{T}$. This, in turn, supports the conclusion that *no* critical wetting transition occurs on the metastable extension of the (l/l/v) coexistence line.

This remarkable conclusion is, on the one hand, in contrast with the experimental observations in the few binary metallic wetting systems studied so far. In Ga-Pb and Ga-Tl, Wynblatt, Chatain et al.[11,52] estimated a value for $\mathcal{T}_{\rm W}$ significantly below the corresponding monotectic temperatures $\mathcal{T}_{\rm M}$, but still at final values of the order of $0.3 \cdot \mathcal{T}_{\rm C}$ and $0.2 \cdot \mathcal{T}_{\rm C}$ for Ga-Pb and Ga-Tl, respectively. On the other hand, it reflects the general finding that in binary metallic systems with short-range interactions the critical wetting transition occurs at significantly lower temperatures than in organic liquid systems, where $\mathcal{T}_{\rm W}$ is found to lie above $0.5 \cdot \mathcal{T}_{\rm C}$. The estimates above indicate that this tendency seems to be driven to its extreme in the case of Ga-Bi: $\mathcal{T}_{\rm W} = 0 \cdot \mathcal{T}_{\rm C} = 0K$.

A semiquantitative argument for the absence of a critical wetting transition in Ga-Bi as compared to the two other metallic systems investigated so far might relate to the fact that in comparison with the others the liquid/liquid coexistence region for GaBi system is significantly shifted towards the Ga-rich, high surface tension end of the phase diagram and, in addition, the miscibility gap is much narrower. As a result, the change in concentration across the l/l interface is smaller for the GaBi system than for the others. In view of the fact that one can express

$$\gamma_{\rm ll} = \kappa \int dz \frac{dc(z)}{dz}^2 \approx \kappa \left(\Delta c\right)^2 \tag{12}$$

this suggests that $\gamma_{\rm ll}$ could be expected to be smaller for GaBi than for the others. If this effect is important, and if it is not compensated by an accompanying reduction in the value of Γ, then it is possible that $\Theta(\mathcal{T}) = \Gamma - \gamma_{\rm ll} > 0$ for all temperatures, thereby precluding a wetting transition.

C. The interplay between tetra point wetting and surface freezing

We would like to point out that the observed wetting of the surface at the GaBi monotectic point by the Bi rich liquid is not necessarily the only phenomenon that can occur. In principle one expects at this tetra point a wetting phenomenology similar to or even more diverse than that predicted[63] and found[64] in the proximity of a triple point in one-component systems. For example, it is also possible for the surface to be wet not by the Bi-rich liquid, but by another one of the coexisting phases, the solid Bi. In the bulk both solid Bi and the Bi rich liquid are stable for $T > T_{\rm M}$; however, for $T < T_{\rm M}$ the free energy of the Bi-rich liquid is larger than that of solid Bi. Consequently, if the solid Bi surface phase had a positive spreading energy it would certainly wet the free surface for $T < T_{\rm M}$. In fact, on the basis of optical and surface energy measurements Turchanin et al.[65,66] proposed a surface phase diagram for which a surface frozen phase of solid Bi forms at the free surface of the GaBi liquid for temperatures below $T_{\rm M}$. Unfortunately, we have several problems with this suggestion. The first problem may be purely semantic, but the idea of a "surface frozen phase" originates in the experiments by Earnshaw et al. and Deutsch, Gang, Ocko et al[67,68] on the appearance of solid surface phases at temperatures above that of bulk freezing for alkanes and related compounds. For the GaBi system the crystalline phase of bulk Bi is stable at temperatures well above those at which Turchanin et al made their observations. We believe that if their observations do correspond to thermal equilibrium phenomena, the effect would be more appropriately described as wetting of the free surface by solid Bi. The second problem is that it is hard to believe that surface wetting by solid Bi is favored by the spreading energy. If wetting by solid Bi were favored, as implied by Turchanin et al, then the wetting layer of Bi-rich liquid, the subject of this paper, would have to be metastable, existing only because of a

kinetic barrier to the nucleation of the solid wetting film. In fact we have regularly observed that on cooling below $T_{\rm M}$ the original fluid, smooth, highly reflecting surfaces became both rough and rigid. The effect is exacerbated by the presence of temperature gradients and by rapid cooling. We interpreted this as the formation of bulk solid Bi, rather than wetting, since we never saw any direct evidence for the formation of films, rather than bulk Bi. We argue that if there is not enough time for the excess Bi in the bulk liquid phase below the surface to diffuse, and precipitate as bulk solid Bi at the bottom of the liquid pan, the bulk liquid would simply undergo bulk spinodal phase separation. This is consistent with our observations. Unfortunately it is very difficult to absolutely prove that our films are stable and this issue can't be resolved from the existing evidence. Nevertheless we find it difficult to understand why solid Bi would wet the surface for $T < T_{\rm M}$ and not wet the surface as T approaches $T_{\rm M}$ from above.

VII. SUMMARY

We reported here x-ray reflectivity measurements of the temperature dependence of wetting phenomena occurring at the free surface of the metallic binary liquid alloy Ga-Bi when the bulk demixes into two liquid phases, i.e. a Bi-rich and a Ga-rich liquid phase. We characterized with Ångstrom resolution the temperature dependence of the thickness and interfacial profile of the Bi-rich wetting films that form at the free surface of the liquid on approaching the (l/l/v) coexistence triple line, i.e. along a path of complete wetting . The results show large concentration gradients in agreement with density functional calculations for such transitions at hard walls. The measurements allowed to determine the short-range surface potential that favors the Bi-rich phase at the free surface and hence is governing the wetting phenomenology. The short-range *complete wetting* transition turns out to be only marginally affected by thermal fluctuations. According to renormalization group analysis the *critical wetting* transition should be more sensitive to critical fluctuations; however, according to our analysis the wetting layer of the Bi rich liquid should be present at all temperatures, and no wetting transition exists. This is in contrast with the results obtained for the two other binary liquid metal systems which were studied. For these the wetting transition were concluded to exist, but could not be observed directly since the metastable l/l/v line falls below the liquidus line.

The largest thickness of the gravitationally limited Bi rich wetting layers that formed at the free surface at (l/l/v)-coexistence were typically of the order of ≈ 50 Å. As a result of the fortuitous balance between the surface potential that favors the Bi-rich Phase and the gravitational potential which favors the lighter Ga-rich phase the interface dividing the two coexisting phases is sufficiently close to the free surface that x-ray reflectivity was sensitive to its microscopic structure. Our measurements were interpreted within a Landau-type square gradient phenomenological theory from which it was possible to extract the sole free parameter of that model, i.e. the influence parameter κ. To the best of our knowledge this is the first time that such a parameter has been directly determined from measurements. Furthermore, it was possible to distinguish between the intrinsic width of the interface and the extra broadening due to thermally-excited thermal capillary waves. Making use of published bulk thermodynamic data, along with the extracted influence parameter, we were able to calculate the (l/l) interfacial tension for a wide temperature range. This quantity is extremely difficult to measure directly, and is not available for Ga-Bi. As a test of our methods we performed the same calculation for the (l/l) interfacial tension in Ga-Pb mixtures, which has a very similar phase behavior to that of Ga-Bi, and for which the (l/l) interfacial tension is available in the literature We assumed that the influence parameter, κ, as determined from our measurements on the (l/l) interfacial structure in Ga-Bi, was also applicable to Ga-Pb and, using the thermochemical data sets available for Ga-Pb, we obtained good agreement between our calculated values and macroscopic measurements of the (l/l) interfacial tension. This suggests that the value of the influence parameter extracted in this study might provide a reasonable value for a larger class of binary metallic alloys. If this proves to be true, the values determined here can be used, along with the surface potential, to predict the wetting properties of this larger class of systems.

Acknowledgments

We thank Prof. S. Dietrich and Prof. B. I. Halperin for helpful discussions. This work is supported by U.S. DOE Grant No. DE-FG02-88-ER45379, National Science Foundation Grant DMR-0124936, and the U.S.-Israel Binational Science Foundation, Jerusalem. BNL is supported by U.S. DOE Contract No. DE-AC02-98CH10886. Patrick Huber acknowledges support from the Deutsche Forschungsgemeinschaft.

APPENDIX: BULK THERMODYNAMICS

Here, we focus on the part of the phase diagram dominated by the miscibility gap and the monotectic point M. In a liquid-liquid (l/l) coexistence of a binary systems, made up of a fixed number of moles of Ga and Bi at a constant atmospheric pressure p and temperature $\mathcal{T}$, the compositions $c_{\rm I}$, $c_{\rm II}$ of the two coexisting bulk liquid phases (I and II) are given by the thermodynamic conditions:

$$\mu^{\rm I}_{\rm Ga}(\mathcal{T}) = \mu^{\rm II}_{\rm Ga}(\mathcal{T}) \quad \mu^{\rm I}_{Bi}(\mathcal{T}) = \mu^{\rm II}_{\rm Bi}(\mathcal{T}) \qquad \text{(A.1)}$$

where μ is the chemical potential. The Gibbs free energy G of the system is:

$$G = U - \mathcal{T}S + PV \quad (A.2)$$
$$G = n\,g = n_{\rm Ga}\,\mu_{\rm Ga} + n_{\rm Bi}\,\mu_{\rm Bi} \quad (A.3)$$

Since the total number of mols $n = n_{\rm Ga} + n_{\rm Bi}$ is constant and only two components have to be considered, the system can be expressed in terms of a molar Gibbs Free Energy, $g(c,\mathcal{T})$, which depends only on the molar fraction c of one of the components:

$$G = n\,(c\,\mu_{\rm Ga} + (1-c)\,\mu_{\rm Bi}\,) \quad (A.4)$$
$$\Rightarrow g(c,\mathcal{T}) = c\,\mu_{\rm Ga} + (1-c)\,\mu_{\rm Bi} \quad (A.5)$$

With this notation the phase equilibrium conditions (equation (A.1) transform into the following two equations:

$$\frac{\partial g}{\partial c}|_{c^{\rm I}} = \frac{\partial g}{\partial c}|_{c^{\rm II}}$$
$$\frac{\partial g}{\partial c}|_{c^{\rm I}} = \frac{g(c^I) - g(c^{II})}{c^I - c^{II}} \quad (A.6)$$

Having a model for the free energy of a binary system, it is possible, then, to calculate $c_{\rm I}$ and $c_{\rm II}$ of the coexisting phases by solving Eqs. (A.6). The standard approach to the description of a miscibility gap in a binary demixing system is the regular solution model for the Gibbs free energy[69]. The resulting miscibility gap has a symmetric shape and is centered around the consolute point $c_{\rm crit} = 0.5$ in the $(c,\mathcal{T})$-plane, quite in contrast to the miscibility gap of Ga-Bi which has an asymmetric shape, and is centered around $c_{\rm crit}$=0.7 in the $(c,\mathcal{T})$-plane. It is necessary, therefore, to resort to an *extended* regular solution model. Relying on data sets for Ga-Bi from the Calphad initiative[15], we use a model based on the Redlich-Kister polynomials $L_\nu(\mathcal{T})$[70,71] and express $g(c,\mathcal{T})$ as:

$$g(c,\mathcal{T}) = c\cdot g_0(Ga)(c,\mathcal{T}) + (1-c)\cdot g_0(Bi) + R\cdot\mathcal{T}\,[\,c\,ln(c) + (1-c)\,ln(1-c)] + \Delta g_{\rm mix}(c,\mathcal{T}) \quad (A.7)$$
$$\Delta g_{\rm mix}(c,\mathcal{T}) = c(c-1)\sum_{\nu=1}^{5} L_\nu(\mathcal{T})(1-2c)^\nu$$

The first two terms correspond to the Gibbs energy of a mechanical mixture of the constituents; the second term corresponds to the entropy of mixing for an ideal solution, and the third term, $\Delta g_{\rm xs}$ is the so-called excess energy term, which is expressed here by a sum of Redlich-Kister polynomials, $L_\nu(\mathcal{T})$, listed in Table II. By solving the nonlinear equations (A.6) for $g(c,\mathcal{T})$ in the temperature range $T_{\rm M} < T < 262°C$ we calculated the binodal coexistence line plotted in Fig. 1. The agreement of the calculated phase boundaries with Predel's measured phase boundaries is excellent. In particular, the measured consolute point C ($T_{\rm C} = 262°$C, $c_{\rm crit} = 0.7$) is very well reproduced by the calculated critical values $T_{\rm C} = 262.8°$C and $c = 0.701$. Furthermore, once $g(c,\mathcal{T})$ is known the binodal lines can be extrapolated below $T_{\rm M}$ into the region of the metastable (l/l) coexistence, and obtain information on the energetics of the metastable Ga-rich and Bi-rich phases. We have also calculated the phase boundaries below $T_{\rm M}$, following the procedure detailed above. For this we used the Gibbs free energy data of pure solid Bi, which coexists for $T < T_{\rm M}$ with a Ga-rich liquid.

ν	Redlich-Kister polynomial $L_\nu(T)$
0	80000-3389+ $\mathcal{T}$
1	-4868-2.4342 $\cdot\mathcal{T}$
2	-10375-14.127 $\cdot\mathcal{T}$
3	-4339.3
4	2653-9.41 $\cdot\mathcal{T}$
5	-2364

TABLE II: Redlich-Kister polynomials used to model the (l/l) miscibility gap of Ga-Bi[15,70].

* Electronic address: p.huber@physik.uni-saarland.de; present address: Fakultät für Physik und Elektrotechnik, Universität des Saarlandes, 66041 Saarbrücken, Germany

[1] J. W. Cahn, J. Chem. Phys. **66**, 3667 (1977).
[2] C. Ebner and W. F. Saam, Phys. Rev. Lett. **38**, 1486 (1977).
[3] P. G. de Gennes, Rev. Mod. Phys. **57** ,827(1985).
[4] D. E. Sullivan and M. M. T. da Gama, *Fluid Interfacial Phenomena*, edited by C. A. Croxton (Wiley, New York), (1986).
[5] S. Dietrich, in C. Domb and J. L. Lebowitz (Eds.), Phase Trans. and Crit. Phen., Vol. 12, Acad. Press, NY, 1988.
[6] B. M. Law, Progress in Surface Science **66**, 159 (2001).
[7] D. Bonn, D. Ross, Rep. Prog. Phys. **64**, 1085 (2001).
[8] A. Plech, U. Klemradt, M. Huber, J. Peisl, Europhys. Lett. **49**, 583(2000).
[9] H. Tostmann, E. DiMasi, O. G. Shpyrko, P. S. Pershan, B. M. Ocko, M. Deutsch, Phys. Rev. Lett. **84**, 4385 (2000).

[10] M. L. Schlossman, Curr. Opinion Coll.&Interf. Sc. **7**, 235 (2002).
[11] D. Chatain and P. Wynblatt, Surface Science **345**, 85 (1996).
[12] H. Shim, P. Wynblatt, D. Chatain, Surface Science **476**, L273 (2001).
[13] D. Nattland, P. D. Poh, S. C. Müller, W. Freyland, J. Phys. C **7**, L457 (1995).
[14] P. Predel, Z. f. Phys. Chemie Neue Folge **24**, 206 (1960).
[15] The calculations of the phase boundaries rely on data sets for Ga-Bi from the CalPhaD initiative (Larry Kaufman (MIT)), which have been refined in order to more accurately reproduce Predel's phase diagram[14].
[16] J. H. Perepezko, C. Galang, K. P. Cooper in G. E. Rindone (ed.), Materials Processing in the Reduced Gravity Environment of Space, Elsevier (Amsterdam) p 491 (1982).
[17] N. Lei, Z. Q. Huang, and S. A. Rice, J. Chem. Phys. **104**, 4802 (1996).
[18] S. Dietrich and M. Schick, Surface Science **382**, 178 (1997).
[19] P. Huber, O. G. Shpyrko, P. S. Pershan, B. M. Ocko, E. DiMasi, M. Deutsch, Phys. Rev. Lett. **89**, 035502 (2002).
[20] M. J. Regan, P. S. Pershan, O. M. Magnussen, B. M. Ocko, M. Deutsch, L. E. Berman, Phys. Rev. B **55**, 15874 (1997).
[21] P. S. Pershan and J. Als-Nielsen, Phys. Rev. Lett. **52**, 759 (1984).
[22] P. S. Pershan, Phys. Rev. E **50**, 2369 (1994).
[23] P. S. Pershan, Coll. Surf. A **171**, 149 (2000).
[24] M. Deutsch and B. M. Ocko in *Encyclopedia of Applied Physics*, G. L. Trigg (ed.) (VCH, New-York, 1998), Vol. 23, p. 479.
[25] M. Tolan, *X-Ray Scattering from Soft-Matter Thin Films*, Springer Tracts in Modern Physics **148** (1998).
[26] L. G. Parratt, Phys. Rev. **95** 358 (1954).
[27] B.M. Ocko, X. Z. Wu, E. B. Sirota, S. K. Sinha, O. Gang, and M. Deutsch Phys. Rev. E**55**, 3164 (1997).
[28] R. Lipowsky, D. A. Huse, Phys. Rev. Lett. **57**, 353 (1986).
[29] X. L. Wu, M. Schlossman, C. Franck, Phys. Rev. B **33**, 402 (1986).
[30] D. Fenistein, D. Bonn, S. Rafai, G. H. Wegdam, J. Meunier, A.O. Parry, M.M. Telo da Gama, Phys. Rev. Lett. **89**, 096101 (2002).
[31] H. T. Davis, *Statistical Mechanics of Phases, Interfaces, and Thin Films*, Wiley-VCH, NY (1996).
[32] F. Schmid, N. B. Wilding, Phys. Rev. E **63**, 031201 (2001).
[33] A. Plech, U. Klemradt, J. Peisl, J.Phys. C **13**, 5563 (2001).
[34] D. Fenistein, D. Bonn, S. Rafai, G. H. Wegdam, J. Meunier, A. O. Parry, M. M. Telo da Gama, Phys. Rev. Lett. **89**, 096101 (2002).
[35] N. W. Ashcroft, Phil. Trans. R. Soc. Lond. A **334**, 407 (1991).
[36] B. Pluis, T. N. Taylor, D. Frenkel, J.F. van der Veen, Phys. Rev. B **40** 1353 (1989).
[37] J. D. van der Waals, Z. Phys. Chem. **13** (1894).
[38] J. W. Cahn, J. E. Hilliard, J. Chem. Phys. **28**, 258 (1958).
[39] S. A. Safran, *Statistical Thermodynamics of Surfaces, Interfaces, and Membranes*, Frontiers in Physics, ed. David Pines, Westview Press (1994).
[40] S. Enders, K. Quitzsch, Langmuir **14**, 4606 (1998).
[41] F. P. Buff, R. A. Lovett , F. H. Stillinger, Phys. Rev. Lett. **15** 621 (1965).
[42] J. S. Rowlinson, B. Widom, *Molecular Theory of Capillary*, Clarendon Press, Oxford (1982).
[43] B. M. Ocko, X. Z. Wu, E. B. Sirota, S. K. Sinha, M. Deutsch, Phys. Rev. Lett. **72**, 242 (1994).
[44] R. K. Heilmann, M. Fukuto, P. S. Pershan, Phys. Rev. B **63**, 205405 (2001).
[45] A. Braslau, P. S. Pershan, G. Swislow, B. M. Ocko, J. Als-Nielsen, Phys. Rev. A **38**, 2457 (1988).
[46] T. Wadewitz, J. Winkelmann, Phys. Chem. Chem. Phys. **1**, 3335 (1999).
[47] R. Evans, Mol. Physs **42**, 1169 (1981).
[48] J. Daillant, A. Gibaud, *X-Ray and Neutron Reflectivity: Principles and Applications*, Lecture Notes in Physics, Springer (1999).
[49] D. Stauffer, M. Wortis, M. Ferer, Phys. Rev. Lett. **29**, 345 (1972).
[50] H. Kreuser and D. Woermann, J. Chem. Phys. **98**, 7655 (1993).
[51] M. Merkwitz, J. Weise, K. Thriemer, W. Hoyer, Zeitschrift für Metallkunde **89**, 247 (1998).
[52] P. Wynblatt, A. Saul, D. Chatain, Acta Metallurgica **46**, 2337 (1998).
[53] I. Ansara, F. Ajersch J. Phase Equilibria **12**, 73 (1991).
[54] P. M. W. Cornelisse, C. J. Peters, J. de Arons, J. Chem. Phys. **106**, 9820 (1997).
[55] S. Fisk, B. Widom, J. Chem. Phys. **50**, 3219 (1969).
[56] J. V. Sengers, J. M. J. vanLeeuwen, Phys. Rev. A **39**, 6346 (1989).
[57] M. Schick, in J. Charvolin, J. F. Joanny, J. Zinn-Justin (Eds.), Liquids at Interfaces, Vol. XLVIII, p. 419.
[58] E. Brezin, B. I. Halperin, S. Leibler, Phys. Rev. Lett. **50**, 1387 (1983).
[59] D. M. Kroll, R. Lipowsky, R. K. P. Zia, Phys. Rev. B **32**, 1862 (1985.)
[60] K. B. Khokonov, S. N. Zadumkin, Sov. Electrochem. **10**, 865 (1974).
[61] A. H. Ayyad, W. Freyland, Surf. Science **506**, 1 (2002).
[62] A. H. Ayyad, I. Mechdiev, W. Freyland, Chem. Phys. Lett. **359**, 326 (2002).
[63] R. Pandit, M.E. Fisher, Phys. Rev. Lett. **51** 1772 (1983).
[64] G. Zimmerli, M. H. W. Chan, Phys. Rev. B **45**, 9347 (1992).
[65] A. Turchanin, D. Nattland, W. Freyland, Chem. Phys. Lett. **337**, 5 (2001).
[66] A. Turchanin, W. Freyland, D. Nattland, Phys. Chem. Chem. Phys. **4**, 647 (2002).
[67] J. C. Earnshaw, C. J. Hughes, Phys. Rev. A **46**, R4494 (1992).
[68] X. Z. Wu, E.B. Sirota, S. K. Sinha, B. M. Ocko, M. Deutsch, Phys. Rev. Lett. **70**, 958 (1993) ; X. Z. Wu, B. M. Ocko, E. B. Sirota, S. K. Sinha, M. Deutsch, G. H. Cao and M. W. Kim, Science **261**, 1018 (1993) ; B.M. Ocko, X. Z. Wu, E. B. Sirota, S. K. Sinha, O. Gang, and M. Deutsch Phys. Rev. E **55**, 3164 (1997) ; O. Gang, X.Z. Wu, B.M. Ocko, E.B. Sirota, and M. Deutsch Phys. Rev. E **58**, 6086 (1998)
[69] P. W. Atkins, *Physical Chemistry*, W.H. Freeman (2001).
[70] U. R. Kattner, JOM-J. Minerals Metals& Mat. Soc. **49**, 14 (1997).
[71] H. L. Lukas, J. Weiss, and E.-Th. Henig, CALPHAD, **6** 229 (1982).
[72] D. Maede, B. S. Haran, R. E. White, MapleTech **3**, 85 (1996).
[73] Additionally, the (s/l/v) triple line due to the coexistence of a Bi-rich liquid, a pure Bi solid, and the vapor phase on the left hand side of the (c,T) phase diagram (Fig. 1) also starts at M. Since it is not relevant to the surface wetting thermodynamics discussed here, and for the sake

of simplicity, it is omitted from Fig. 2(a),(b).

[74] We used the standard procedures for solving differential equations included in the *Maple 7* software package (Waterloo Maple Inc.) as well as the *"Shooting Technique for the solution of two-point boundary value problems"* as implemented for this software package by D.B. Maede[72].

[75] Note that the TSFU hypothesis is strictly valid only in a T-range where mapping of the demixing process on a second order phase transition is justified. This is typically the case for $t < 10^{-1}$. In practice, however, TSFU is often found to describe well experimental results over much larger t ranges, e.g the measurements of Merkwitz et al.[51]($t \leq 0.34$) and ours ($t \leq 0.45$)

[76] The largest contribution to the error budget of ξ is due to the uncertainty in assigning a thickness value to the wetting layer from the experimentally-derived, strongly inhomogeneous density profile